ELSEVIER

Earth and Planetary Science Letters 133 (1995) 271–282

EPSL

Detection of inherited monazite in the Manaslu leucogranite by $^{208}Pb/^{232}Th$ ion microprobe dating: Crystallization age and tectonic implications

T. Mark Harrison [a], K.D. McKeegan [a], P. LeFort [b]

[a] *W.M. Keck Foundation Center for Isotope Geochemistry, Department of Earth and Space Sciences and Institute of Geophysics and Planetary Physics, University of California, Los Angeles, CA 90024, USA*

[b] *Institut Dolomieu, C.N.R.S., Grenoble, 38301, France*

Received 10 January 1995; revised 11 May 1995; accepted 16 May 1995

Abstract

Although leucogranites are among the least petrologically variable of all igneous rocks, ironically they are among the most difficult to reliably date. The High Himalayan leucogranites have been the subject of numerous geochronological investigations because of their interrelationship with the most significant tectonic features of that mountain belt. For a variety of reasons linked to the minimum melt composition of these leucogranites, these dating studies have not been entirely successful. We report results of a new ion microprobe dating method based on the decay of ^{232}Th to ^{208}Pb in monazite that has directly revealed the presence of inherited Pb in monazite from the Manalsu granite, casting doubt on its previously accepted age. Monazite ages obtained from this leucogranite yield two distinct populations, a large number of ages with a normal distribution and mean age of 22.4 ± 0.5 Ma (± 2 S.E.) that we interpret to be the crystallization age, and a smaller inherited fraction with an age of ca. 600 Ma. Because formation of the granite is thought to be related to slip on the Main Central Thrust, both this date and a second less precise result from a structurally similar pluton near Mt. Everest indicate that the Main Central Thrust was active in the interval 24–22 Ma, but do not constrain its initiation. Together with crosscutting relationships, these data require that movement on the North Himalayan Fault occurred prior to 22 Ma at both locations.

1. Introduction

The High Himalayan leucogranites, a discontinuous chain of about a dozen plutons extending 2000 km along the crest of the Himalaya (Fig. 1), have been the focus of repeated geochronological studies because of their interrelationship with the most significant tectonic features of that mountain belt [1]. The Manaslu granite (Fig. 1), the most thoroughly studied of these intrusions [1–14], is emplaced into and cuts a north-verging recumbent anticline developed within low-grade Tethyan metasediments. The base of that fold is delineated by the North Himalayan Fault (NHF) (also called the South Tibetan Detachment), a down-to-the-north, low-angle normal fault traceable the length of the Himalayan front [15–18]. Although Manaslu leucogranites clearly cut the NHF, the development within the pluton of both a pervasive fabric and localized ductile normal faulting with a right lateral component indicates that internal deformation was occurring while the leucogranite was still at high temperature [10,13]. Beneath the NHF are schists and gneisses of the Greater Himalayan Crystallines that are themselves

SSDI 0012-821X(95)00091-7

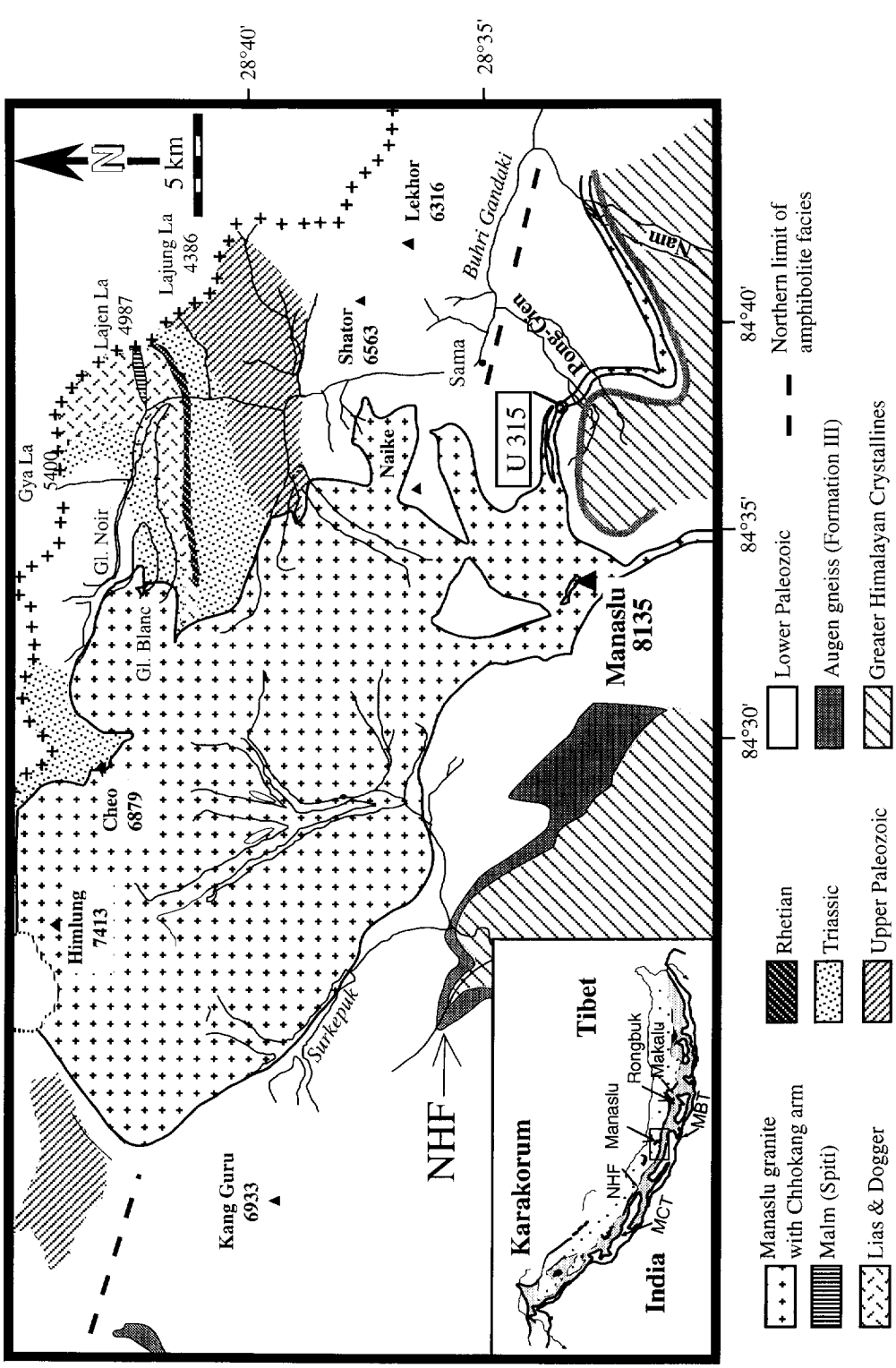

Fig. 1. Geological map of the Manaslu region showing the intrusive relationship of the granite into Tethyan metasediments. The Greater Himalayan Crystallines are juxtapos adjacent these rocks by the North Himalayan Fault (*NHF*). The inset is a sketch map of the Himalaya showing the location of the geological map, Rongbuk and Makalu granites, the Main Central Thrust (*MCT*), Main Boundary Thrust (*MBT*) and NHF. The High Himalayan Leucogranites are shown in the inset in black.

juxtaposed atop lower-grade schists of the Lesser Himalayan Formations by the Main Central Thrust (MCT), a south-directed fault thought to be responsible for early thickening of the Himalaya [1–13] (Fig. 2). The High Himalayan leucogranites are generally interpreted [1–9] to be the product of anatexis in the Greater Himalayan Crystallines following infiltration of fluids evolved from the Lesser Himalayan Formations during thrusting along the MCT (Fig. 2).

The tectonic importance of these leucogranites is twofold. Because anatexis appears to be related to devolatilization of the footwall during thrusting [1–9], crystallization ages provide a constraint on the timing of slip on the MCT. Geochronology of rocks adjacent to the MCT shear zone suggests that it was active prior to 21 Ma [19,20], but the earlier history of thrusting is poorly understood. Secondly, the NHF both cuts, and is cut by, various of the High Himalayan leucogranites [15,17,18]. Establishing the age(s) of emplacement of these intrusions would constrain both upper and lower bounds on the movement of the NHF. However, a variety of effects, largely related to the minimum melt character of these petrologically simple rocks, have complicated attempts to obtain accurate crystallization ages. Extremely heterogeneous $^{87}Sr/^{86}Sr$ and $^{143}Nd/^{144}Nd$ initial ratios of the granites [1], probably a result of emplacement by dyke intrusion rather than a process that would cause thorough mixing and isotopic equilibration of the magma [21], effectively precludes whole rock isochron dating. High ambient temperatures [11], the presence of excess argon [11,12], and the absence of magmatic hornblende seriously limit the use of $^{40}Ar/^{39}Ar$ dating in this environment. In addition to the relative youth of the High Himalayan leucogranites, which minimizes advantages of the concordia plot, U–Pb accessory mineral dating is complicated by several geochemical controls. Solubilities, and thus abundances, of these phases are very low in leucogranite magmas [22,23] and the likelihood of their containing an inherited component is therefore very high [24]. Although monazite has the advantage of being less refractory during orogenesis than zircon, it commonly incorporates ^{230}Th (an intermediate daughter in the decay chain of ^{238}U) during crystallization [25] and as a result contains unsupported radiogenic ^{206}Pb ($^{206}Pb^*$).

Attempts to determine the age of the Manaslu granite have encountered all of the problems described above. Manaslu whole rock Sr and Nd initial ratios are extremely variable precluding isochron relationships [8,9], although Deniel et al. [9] found about two-thirds of the samples obtained from one continuous outcrop yielded a Rb–Sr isochron age of 18.1 ± 0.5 Ma. The same workers found one leucogranite sample that contained sufficient monazite for U–Pb analysis but only enough for a single measurement. As expected, the sample contained unsupported $^{206}Pb^*$ with $^{206}Pb/^{238}U$ and $^{207}Pb/^{235}U$ ages of 26.6 and 25.7 Ma, respectively. Nevertheless, on the basis of their Rb–Sr and U–Pb results, Deniel et al. [9] suggested that magmatic

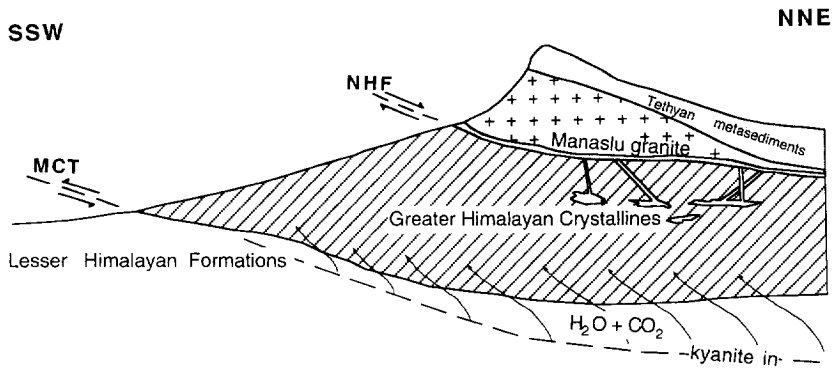

Fig. 2. Schematic cross-section through the High Himalaya showing the inferred relationships between motion on the Main Central Thrust (*MCT*), devolatilization of the Lesser Himalayan Formations, and subsequent anatexis of the Greater Himalayan Crystallines. Also shown are the network of dykes feeding the leucogranite pluton which crosscuts the North Himalayan Fault (*NHF*) and intrudes into Lower Paleozoic to Jurassic metasediments (adapted from [1]).

activity began at ~25 Ma and lasted for 7 Myr. Subsequently, Copeland et al. [24] discovered (in sample D33 from the Rongbuk granite near Mt. Everest; Fig. 1) that monazite can retain inherited Pb^* at anatectic temperatures and cautioned against relying on a single result for age interpretation. Because the inherited Pb^* discordia defined by the $\Delta 33$ data [24] passes through the result of Deniel et al. [9], it was later argued that the Manaslu granite was more likely similar in age to that estimated for the Rongbuk granite [11].

2. $^{208}Pb/^{232}Th$ ion microprobe dating of monazite

The high-sensitivity/high-resolution ion microprobe has been used successfully for over ten years to date zircon by the U–Pb method [26]. We have developed a similar methodology that permits precise (±2%) Th–Pb dating of Tertiary monazites using a CAMECA ims 1270 ion microprobe. The $^{208}Pb/^{232}Th$ system has several advantages over U–Pb in dating monazite. Because secular equilibrium among the intermediate daughter isotopes of ^{232}Th is attained within ~30 yr, it is highly unlikely that monazite could contain unsupported $^{208}Pb^*$. Thorium concentrations are very high in monazite, typically between 3 and 8% [23], therefore resulting in high levels of $^{208}Pb^*$. Coupled with the relatively high ionization efficiency of Pb from monazite, this highly radiogenic signal allows an age determination to be made in a 10×15 μm spot on a Tertiary specimen in ~15 min.

We surveyed experimental conditions to determine an operating mode for the ion microprobe which optimized Pb sensitivity while yielding reproducible inter-element ratios. All results reported here are on monazite grains mounted in epoxy, polished to 0.3 μm alumina, and coated with ~100 Å of Au using a sputter-coater. The standard operating conditions used for analyses presented in this paper are: O^- primary beam focused to a $\sim 10 \times 15$ μm spot, a mass resolving power (MRP) of about 4500, a 50 eV energy window, and a 15 eV offset for $^{232}Th^+$.

Molecular ions in the 204–208 mass range have the potential to interfere with the Pb peaks requiring the use of high MRP. High-resolution mass spectra

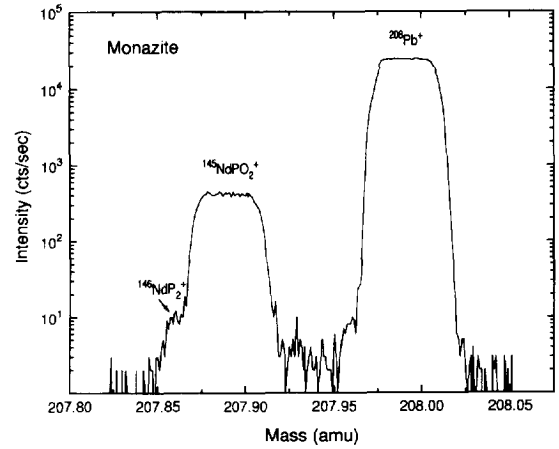

Fig. 3. Measured ion intensity plotted as a function of mass in this high-resolution spectrum of the mass 208 region from monazite 83-32. Molecular ion interferences are well separated from the $^{208}Pb^+$ peak with a mass resolving power (MRP) of ~4500. This MRP is sufficient to resolve all significant molecular interferences [primarily $(Nd,Pr)PO_2^+$] from the other Pb isotopes as well.

of natural monazites show that the principal interferences are mostly $LREE(PO_2)^+$, for example $^{145}NdPO_2^+$ at mass 208 and $^{141}PrPO_2^+$ at mass 204 (Fig. 3). These molecular interferences can be completely separated from the Pb isotopes at an MRP of only about 4500, compared to ~6000 to resolve $HfSi^+$ in zircon [26]. The possibility that unresolved interferences exist at the exact masses of the Pb peaks in monazite was tested using a synthetic Nd-monazite grown in a hydrothermal environment free of Pb [27]. Under our standard analysis conditions, mass spectra show low or zero ion intensities at the positions corresponding to the Pb masses (e.g., mass 204, Fig. 4). Although the small signals inhibit precise measurement, Pb isotope ratios of this background are consistent with that of common Pb, leading us to conclude that this component is derived from surface contamination and that no measurable molecular interferences exist at the Pb masses for an MRP = 4500. Interferences in compositionally more complex natural monazites are possible, but the low dispersion of calculated ages suggest they are not significant. Tests using Moacir monazite (Pb = 1470 ± 130 ppm; J.M. Montel, pers. commun.) indicate ion yields of up to 40 cps/ppm Pb/nA for primary ion beams of < 5 nA.

Although ion microprobe measurements of Pb

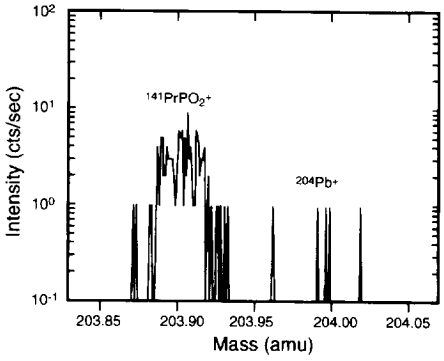

Fig. 4. Mass spectrum in the vicinity of mass 204 obtained from a hydrothermally-synthesized monazite [27]. Although nominally an endmember Nd-monazite, the principal peak in the spectrum ($^{204}PrPO_2^+$) indicates the presence of minor amounts of praseodymium. This interference appears to be ubiquitous in natural monazites and is routinely used to determine the position of $^{204}Pb^+$ which is found 0.1018 amu to the high mass side of the $^{204}PrPO_2^+$.

isotopes in zircons have not revealed a measurable isotopic discrimination [26], we wished to test whether Pb is fractionated during sputtering from monazite. To assess this, we analyzed Pb isotopes from a Pr-monazite synthesized in a lead orthophosphate flux [28]. A mm-sized grain of this sample was heated at 210°C in an HF–HCl solution for three weeks after which three aliquots of the solution were measured for Pb isotopes by thermal ionization mass spectrometry (TIMS). Triplicate TIMS measurements, corrected for fractionation using a discrimination factor derived from measurements of NBS 981 under identical instrumental conditions, yield $^{208}Pb/^{206}Pb = 2.087 \pm 0.001$ and $^{207}Pb/^{206}Pb = 0.8636 \pm 0.0017$. This result is in excellent agreement with three ion microprobe measurements which yield $^{208}Pb/^{206}Pb = 2.086 \pm 0.004$ and $^{207}Pb/^{206}Pb = 0.8645 \pm 0.0008$. Therefore, we conclude that under our standard measurement conditions, instrumental mass discrimination is less than 1‰/amu.

In contrast to thermal ionization, the sputtering process produces a relatively broad range of ion energies. Fig. 5 shows the distribution of energies for $^{232}Th^+$, $^{248}ThO^+$, $^{264}ThO_2^+$, and $^{208}Pb^+$ ions sputtered from an Archean monazite measured with an energy window of ~ 50 eV. Although it is well known that molecular ion intensities drop off more sharply at higher energies compared to elemental ions, our earlier observation that Pb^+ sputtered from zircon has an energy dependence comparable to that of uranium oxide ions [29] is also true of monazite (Fig. 5). Because the energy distributions of $^{208}Pb^+$ and $^{264}ThO_2^+$ are similar, but contrast with that for $^{232}Th^+$, we chose to investigate possible correlations between these species as the basis for a Pb/Th calibration. Since the peak intensity of $^{232}Th^+$ is offset by ~ 15 eV from the center of the plateau-like portions of the $^{208}Pb^+$ and $^{264}ThO_2^+$ distributions (Fig. 5), we chose to perform the isotopic measurements using a 15 eV offset for $^{232}Th^+$ to achieve the most stable measurement conditions. We note that the energy spectra across the peak intensities (~ 20–70 eV, Fig. 5) yield a linear array when plotted as $^{264}ThO_2^+/^{232}Th^+$ vs. $^{208}Pb^+/^{232}Th^+$. Thus it is expected that if ion energies change, for example as a result of sample charging during analysis, the resulting displacement to a different position on the energy spectrum will produce a systematic shift to another position along this line.

Under our standard operating conditions, repeated Th–Pb isotopic measurements of an Archean monazite (83-32) yield a linear relationship on a plot of $^{264}ThO_2^+/^{232}Th^+$ vs. $^{208}Pb^+/^{232}Th^+$ (Fig. 6). The linear array defined by these data is similar to the model calibration plot predicted by the energy spectra leading us to conclude that, at least to the first order, variations in Pb/Th ratios result from shifts in

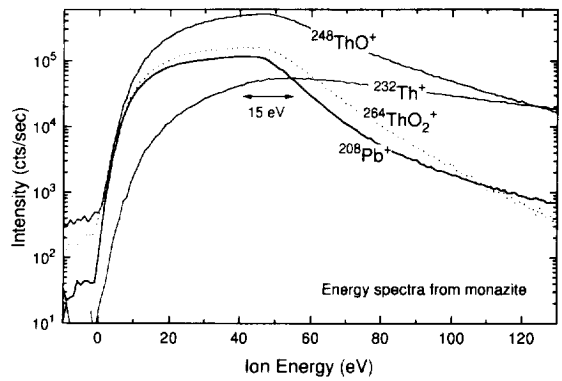

Fig. 5. Plot of the kinetic energy distribution of sputtered ions from monazite measured with a ~ 50 eV energy window. Note that Pb^+ and ThO_2^+ have remarkably similar behavior but both distributions are substantially different from that of Th^+.

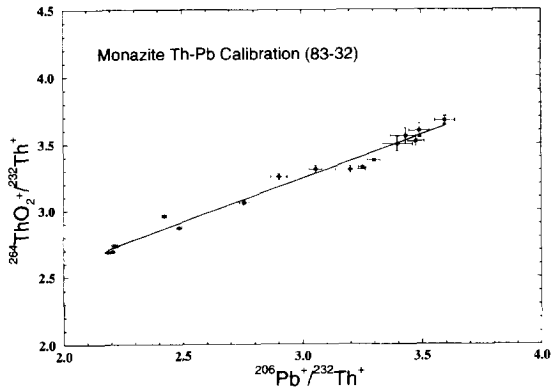

Fig. 6. Plot of $^{264}ThO_2^+/^{232}Th^+$ vs. $^{208}Pb^+/^{232}Th^+$ for monazite standard 83-32 [30] (excluding one highly discordant datum). By using the known age (2685 ± 2 Ma), this relationship allows a relative sensitivity factor to be calculated permitting determination of Pb/Th ratios of unknowns measured under the same conditions. Reproducibility of this calibration is typically ±2%.

ion energy due to sample charging during analysis. The correlation between $^{264}ThO_2^+/^{232}Th^+$ vs. $^{208}Pb^+/^{232}Th^+$, analogous to the $^{254}UO^+/^{238}U^+$ vs. $^{206}Pb^+/^{238}U^+$ relationship found for zircon [26], allows a correction factor to be derived by dividing the measured $^{208}Pb^+/^{232}Th^+$ of a standard monazite at a reference $^{264}ThO_2^+/^{232}Th^+$ value by its known daughter to parent ratio. The age of an unknown, measured under identical conditions, can then be determined by applying this relative sensitivity factor. For ca. 20 Ma monazites, the precision of the method is not limited by counting statistics but by the reproducibility of the calibration curve (e.g., Fig. 6) which is typically ±2%.

We adopted Archean monazites 87-40 and 83-32 as our primary standards ([30]; F. Corfu, pers. commun.). Their U–Pb monazite ages are concordant at 2691 ± 2 Ma and 2685 ± 2 Ma, respectively (all age uncertainties are quoted at ±2 standard error of the mean). Using these materials as standards, we then analyzed several monazites of known age; 87-37 (2670 ± 2 Ma; [F. Corfu, pers. comm.]), 8602-1 (389 ± 1 Ma; [31]) and SW-1 (68.2 ± 0.9 Ma; [32]). Our measurements over a two month period yielded an average dispersion of 1.4% from their known age (Table 1). This result is well within the ±2% standard error of each measurement and includes values that are both higher and lower than the established age indicating that the method is also accurate to this

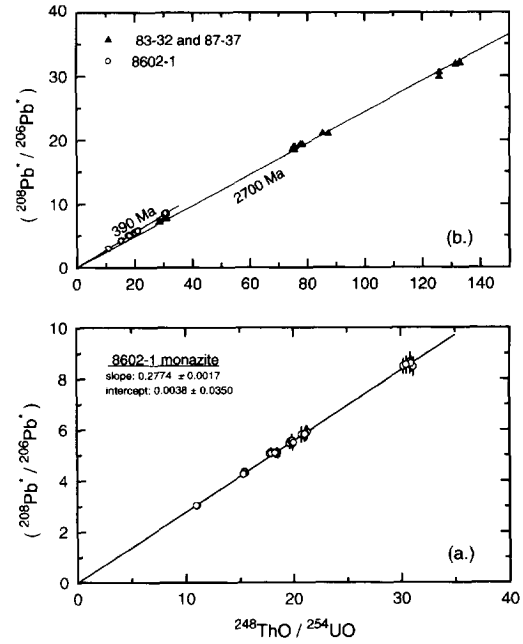

Fig. 7. (a) Plot of $^{208}Pb^*/^{206}Pb^*$ vs. $^{248}ThO^+/^{254}UO^+$ for 8602-1 monazite (389 ± 1 Ma). The linearity of this array indicates that the U–Pb and Th–Pb ages are concordant to within 0.6%. (b) Data for 8602-1 are as in (a) with the 390 Ma isochron indicated. Using this line as a reference from which to calculate the relative sensitivity of Th/U, the predicted isochron for 2700 Ma is shown. The measured data for 83-32 (2685 ± 2 Ma) and 87-37 (2670 ± 2 Ma) yield an excellent fit to the calculated isochron.

level. Although the known ages of our standards are based on U–Pb systematics, the concordancy of their U–Th–Pb systems can be assessed by plotting thorogenic to uranogenic Pb vs. oxides of thorium and uranium (i.e., $^{208}Pb^*/^{206}Pb^*$ vs. $^{248}ThO/^{254}UO$) [26]. For example, the results for 8602-1 monazite (Fig. 7) define an isochron indicating concordancy between U–Pb and Th–Pb ages at the ±0.6% level.

Table 1
Comparison of measured monazite age with independently established values

Sample	Known Age (Ma)	Measured Age (Ma)	Ref.
87-37	2670±2	2696±51	[27]
8602-1	389±1	383±8	[28]
SW-1	68.2±0.9	67.0±1.3	[26]

Note that this uncertainty is substantially lower than the overall uncertainty inherent in our Th–Pb ages. This result is due to the fact that ion microprobe inter-element calibrations are more reproducible for U/Th ratios than for Pb/Th or Pb/U ratios, presumably reflecting the fundamental difference in energy distributions for these ions. Since the slope on this plot is a function of time, we can predict the slope for the ~2700 Ma Archean standards. This calculated line, also shown in Fig. 7, agrees remarkably well with our measured values over a wide range of thorium to uranium ratios.

3. Manaslu granite

Monazite grains of ~50–100 μm size were picked from a heavy concentrate of sample U315, a two-mica + tourmaline leucogranite from near the base of the pluton (84°39′14″/28°34′57″; Fig. 1), and mounted in epoxy together with standard 87-40. Attempts to separate monazite from heavy concentrates of three other samples (U464, U476, and X51) were unsuccessful in that only one or two grains were obtained in each case. Twenty-four of twenty-eight ion microprobe analyses on 18 grains yield a normal distribution of $^{208}Pb/^{232}Th$ ages with a mean of 22.4 ± 0.5 Ma (Fig. 8a; Table 2). The similarity of the weighted mean age of 22.7 ± 0.3 Ma indicates that the distribution of individual ages is consistent with all error being due to analytical uncertainties alone. All monazite ages reported have been corrected for common Pb based on the average Manaslu whole rock $^{208}Pb/^{204}Pb$ ratio of 39.5 ± 0.1 [8]. Radiogenic fractions were typically ~95% for $^{208}Pb^*$, (Table 2) compared to ~90% and ~50% for $^{206}Pb^*$ and $^{207}Pb^*$, respectively. Although the 22.4 ± 0.5 Ma age appears to be supported by ca. 22 Ma $^{40}Ar/^{39}Ar$ hornblende ages from the Manaslu aureole [12], large errors (e.g., 21^{+14}_{-6} Ma) limit the usefulness of these data as constraints on the age of the pluton [33].

Four spots on one grain give $^{208}Pb/^{232}Th$ ages between 614 and 574 Ma indicating the presence of inherited $^{208}Pb^*$ in monazite from the Manaslu granite. The inherited $^{208}Pb/^{232}Th$ component for this grain is confirmed by $^{207}Pb/^{206}Pb$ ages which range from Late Proterozoic to Early Paleozoic. The broad

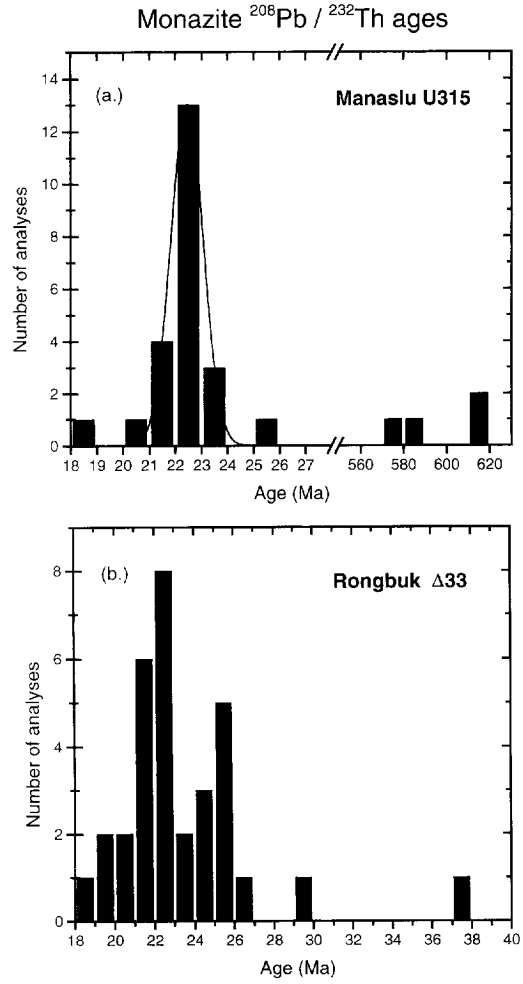

Fig. 8. (a) Histogram of $^{208}Pb/^{232}Th$ ages obtained from ion microprobe spot analyses of monazites from the Manaslu granite. This distribution indicates a crystallization age of 22.4 ± 0.5 Ma (±2 S.E.) and reveals the presence of an inherited component with an age of ~600 Ma. (b) Histogram of $^{208}Pb/^{232}Th$ ion microprobe ages of monazites from the Rongbuk granite which, together with other data, suggest a crystallization age of $22^{+1.0}_{-0.5}$ Ma.

agreement between the $^{208}Pb/^{232}Th$ and $^{207}Pb/^{206}Pb$ ages indicates that relatively little Pb^* loss occurred from this grain during metamorphism, anatexis, and cooling. This suggests that the ages of magmatic monazites, which have only experienced the retrograde history, correspond to the age of crystallization. Assuming that the conventional U–Pb age of ~26 Ma [9] represents the average mixture

of the magmatic plus inherited components present in the Manaslu granite, our endmember ages of 22 and ~600 Ma suggest that only about 1% of the monazite is inherited. This is broadly consistent with our finding one inherited grain among the 18 we examined, or about 5%. Although the presence of inherited $^{208}Pb^*$ in Manaslu potentially complicates the common Pb correction, any adjustments to the final ages are entirely insignificant since we estimate the inherited component to be only 1–5% of the total monazite, and the highly radiogenic magmatic monazites are insensitive to this correction (Table 2).

Copeland et al. [24] first documented evidence of inherited Pb^* in magmatic monazite, but our results using an in-situ technique provide the first direct measurements of the restitic endmember. The ages obtained from the restitic grain are older, but in the same general range, as the upper intercept of the $\Delta 33$ monazite discordia (472 ± 30 Ma) and ages obtained for the Greater Himalayan Crystallines

Table 2
Th–Pb ion microprobe analyses of Manaslu monazite U315

Spot[1]	$^{264}ThO_2/^{232}Th$[2] (±σ)	Standard $^{208}Pb^*/^{232}Th$[3]	$^{208}Pb^*$[4] (%)	$^{208}Pb^*/^{232}Th$[5] (±σ)	Age (Ma) (±σ)[6]
MAN11A	2.784±0.035	2.755	96.1	0.0225±0.0007	23.5±1.1
MAN31A	2.883±0.040	2.869	95.7	0.0256±0.0008	25.6±0.9
MAN44A	3.128±0.045	3.151	94.9	0.0251±0.0007	22.9±0.9
MAN44B	3.021±0.054	3.074	92.2	0.0244±0.0008	22.8±1.0
MAN41A	3.114±0.043	3.188	95.1	0.0248±0.0008	22.4±0.9
MAN32A	2.878±0.023	2.900	94.1	0.0229±0.0006	22.7±0.6
MAN32A2	2.791±0.021	2.794	97.6	0.0225±0.0006	23.1±0.6
MAN32B	2.615±0.027	2.579	95.5	0.0188±0.0008	21.0±1.0
MAN46A	2.819±0.019	2.828	85.2	0.0211±0.0012	21.5±1.2
MAN36A	2.296±0.036	2.237	93.6	0.0170±0.0027	21.9±3.5
MAN36A2	2.228±0.060	2.152	92.5	0.0167±0.0007	22.3±0.9
MAN35A	2.692±0.023	2.730	96.2	0.0224±0.0003	23.6±0.5
MAN35B	2.569±0.023	2.577	94.9	0.0215±0.0003	23.9±0.5
MAN34A	3.102±0.049	3.240	92.5	0.0248±0.0013	22.0±1.2
MAN28A	3.348±0.043	3.547	99.8	0.7665±0.0075	613±50
MAN28B	3.075±0.052	3.207	99.9	0.6485±0.0065	574±15
MAN28C	3.178±0.110	3.335	99.8	0.6864±0.0236	584±29
MAN28D	3.218±0.267	3.385	99.4	0.7331±0.0062	614±51
MAN27A	3.176±0.033	3.333	95.3	0.0258±0.0052	22.3±4.3
MAN26A	2.800±0.032	2.875	95.4	0.0224±0.0004	22.4±0.5
MAN23A	3.160±0.038	3.325	93.7	0.0261±0.0006	22.6±0.5
MAN23B	2.595±0.044	2.619	96.2	0.0169±0.0008	18.6±1.0
MAN22A	3.104±0.040	3.255	79.4	0.0226±0.0020	20.0±1.8
MAN12A	3.140±0.044	3.300	88.9	0.0260±0.0006	22.7±0.5
MAN12B	2.990±0.014	3.113	79.6	0.0227±0.0007	21.0±0.6
MAN13A	2.928±0.023	3.035	91.5	0.0241±0.0006	22.8±0.6
MAN14A	3.027±0.033	3.123	96.3	0.0248±0.0004	22.9±0.5
MAN15A	3.132±0.044	3.290	95.1	0.0255±0.0008	22.3±0.7

[1] The two digit number indicates the row and column, respectively, on the grain mount of the analyzed monazite. Letters distinguish different spots on the same grain.
[2] Measured ratio in sample.
[3] Calculated ratio in monazite standard 87-40. Reproducibility of the calibration is ±2%.
[4] Thorogenic ^{208}Pb assuming initial $^{208}Pb/^{204}Pb = 39.5 \pm 0.1$ [8].
[5] Corrected sample ratio.
[6] Uncertainty calculated by quadratically summing errors in $^{264}ThO_2/^{232}Th$, $^{208}Pb^*/^{232}Th$, and the Pb/Th calibration (i.e., ±2%).

source rock (507 ± 42 Ma) [7,24]. Given the low solubility of monazite in leucogranites [23], it is not surprising that this sample exhibits inheritance. The fact that the age of the inherited component is consistent with previous estimates of the protolith age argues against random laboratory contamination as a source of this grain. Of course it is still possible that the Manaslu granite is heterogeneous with respect to crystallization age, but the documentation of an inherited monazite component in U315 casts considerable doubt on the reliability of the ~ 26 Ma datum of Deniel et al. [9] as representing the crystallization age.

Although the inferred granite source region in the Higher Himalayan Crystallines typically contains > 150 ppm LREE + Th [8], the granite averages only ~ 50 ppm [4]. This is expected because of the limited solubility of monazite in the melt [23]. Using accessory mineral thermometry [22], Montel [23] calculated monazite saturation temperatures for the Manaslu pluton between 680 and 730°C assuming that all LREE present were in solution. Although this assumption is not entirely correct, our estimate that only 1–5% of an inherited monazite component is present in the Manaslu granite does not lead to a significant change to that calculated temperature, which agrees well with empirical [5] and experimental [34] estimates of the peak melting temperature of 700–750°C.

4. Other High Himalayan leucogranites

Thirty $^{208}Pb/^{232}Th$ measurements of monazites from the D33 sample of the Rongbuk granite [24,35] were made using the 83-32 standard. The resulting age distribution is more complex than that for U315 (Manaslu) but also shows a dominant peak near 22 Ma (Fig. 8b). The observed tailing to older ages is expected since we know from the work of Copeland et al. [24] that this sample contains inherited Pb^*. However, a detailed investigation of the age distribution was difficult since the larger and inclusion free grains of this mineral separate were consumed during previous investigations [24,35]. If for the moment we exclude the 8 monazite ages older than 25 Ma as representing an inherited component, the remaining 22 data define a broadly normal distribution with a mean age of 22 ± 1 Ma. Although this cutoff is admittedly arbitrary, several other lines of evidence indicate that this provides a good estimate of the crystallization age for the Rongbuk pluton.

Previous xenotime and low radiogenic (~ 30%) zircon U–Pb dates for Δ33 were interpreted to indicate crystallization at 20.6 ± 0.1 [35] and 20 ± 1 Ma [25], respectively. However, the uncertainty on the zircon age [24] was originally underestimated (R.R. Parrish, pers. commun.) and several monazite $^{207}Pb/^{235}U$ dates (recall that the $^{206}Pb/^{238}U$ ages are problematic) from the same sample cluster between 21.5 and 21.9 Ma [24]. Consistent with this clustering are three additional xenotime ages that range up to 21.6 ± 0.1 Ma [18]. Because inherited Pb^* has not been documented in xenotime, and high-U xenotime may be particularly susceptible to Pb loss [36], we interpret the oldest xenotime (which contains 2% U) date to be a cooling age and thus a minimum estimate of the age of Rongbuk. A crystallization age of the Rongbuk granite of $22^{+1.0}_{-0.5}$ Ma is thus consistent with all the isotopic data obtained on this rock.

Schärer's [25] classic study of a third undeformed leucogranite, the Makalu granite (Fig. 1), explored the effects of ^{230}Th disequilibrium on the monazite U–Pb system, yielding disequilibrium corrected ages of 21.9 ± 0.2 and 24.0 ± 0.4 Ma. Although multiple generations of leucogranite dykes occur within this region, Manaslu and Rongbuk–Makalu taken together represent the majority of leucogranite exposed in the High Himalaya between Mustang and Bhutan [1]. Based on Rb–Sr isochron ages, it was previously thought that the Manaslu pluton formed over a period spanning 29–18 Ma [9,14]. However, monazite Pb^* crystallization ages for the Manaslu, Rongbuk and Makalu granites now appear to be restricted to the range 24.4–21.5 Ma. Although reliable ages have thus far been obtained on only a few samples, the data suggest that a significant phase of anatexis within this portion of the Greater Himalayan Crystallines occurred over a relatively narrow time interval.

5. Tectonic implications

The MCT is thought to be the earliest of the crustal-scale thrusts developed on the Indian conti-

nent along which > 100 km of south-directed displacement occurred [37]. The Gangdese thrust, a south-directed fault in southern Tibet, was active until ~ 24 Ma [38]. Thrust-related melting above the MCT between 24–22 Ma is consistent with the conventional interpretation that the progression of major thrust initiation in the Indo-Asian collision zone has generally been towards the south. The observation of undeformed 22 ± 1 Ma anatectic pods crosscutting MCT-related structures in Nepal [20] potentially restricts this phase of deformation/anatexis to < 3 Myr.

Because the Manaslu granite crosscuts the NHF and a related hanging wall collapse structure, that phase of normal faulting must have ceased there by 22 Ma, and the phase of syn-magmatic oblique-slip normal faulting must have been active some time between 22.9–21.9 Ma. Twenty-five km NNW of Mt. Everest, the NHF (locally termed the Qomolangma detachment) is cut by the Rongbuk granite [17]. Our interpreted age of $22^{+1.0}_{-0.5}$ Ma is consistent with the earlier conclusion of Copeland et al. [39] that motion on the detachment is at least as old as 22 Ma. However, the magnitude of displacement on this detachment [17], together with a liberal estimate of slip rate, is difficult to reconcile with the interpretation of Hodges et al. [17] who judged that all of the fault movement occurred between 22–19 Ma. Guillot et al. [12] inferred a difference of at least 3 Myr in activity of the NHF between the Qomolangma and Manaslu locations based on the Deniel et al. [9] and Hodges et al. [18] chronologies for the Manaslu and Rongbuk granites, respectively. However, that timing of movement on the Qomolangma detachment [18] hinges on both a high-precision estimate of a very low radiogenic sphene–feldspar U–Pb isochron and a range of closure temperatures for metamorphic hornblende (510–540°C) which may be too restrictive given that previous workers have found possible values as low as ~ 300°C [40,41]. Although our determination of the age of the Rongbuk granite is subject to an assumption about the nature of inheritance in this sample, we feel that the balance of evidence (i.e., conventional U–Pb monazite age cluster [24], conventional U–Pb xenotime ages [18,35], and the majority of the ion microprobe Th–Pb monazite ages) currently favors a crystallization age of 22 Ma. This age would suggest that motion on the NHF had terminated by $22^{+1.0}_{-0.5}$ Ma at the two localities thus far dated in the central Himalaya.

The younger bound on NHF activity is therefore reasonably well constrained in the central Himalaya, but there currently are no geochronological data that constrain the earliest phases of motion on this detachment. The paradigm for Himalayan leucogranite petrogenesis is that devolatilization of the Lesser Himalayan Formations, due to slip on the MCT, leads to anatexis in the hanging wall and subsequent intrusion across the NHF. The different causal mechanisms relating thrusting and extension that have been postulated for this orogeny [15–17,42,43] can be evaluated given appropriate timing constraints. For example, Yin [42] showed that the state of stress within a thrust hanging wall is critically dependent on pore-fluid pressure along the fault. Partial melting of the Greater Himalayan Crystallines would provide a sink for volatiles evolved during metamorphism, thereby reducing the pore-fluid pressure along the thrust and creating stress conditions in the hanging wall favorable for normal faulting. Clearly this model requires that MCT motion predate initiation of normal faulting. Although the chronological data permit synchroneity of motion on the NHF and MCT, our estimate of the time required (> 3 Myr) to accommodate the magnitude of slip recognized on the NHF [17] would appear to preclude a genetic link unless the MCT was active prior to 24 Ma.

6. Conclusions

We have developed a new ion microprobe method that permits in-situ Th–Pb dating of young leucogranites with ±2% precision and accuracy. Analyses of monazite from the Manaslu granite reveal the presence of restitic monazite at the percent level. These data permit clear resolution between the magmatic and inherited components and allow an accurate determination of the crystallization age of this pluton at 22.4 ± 0.5 Ma. Thirty measurements of monazite from the Rongbuk granite near Mt. Everest yield a more complex distribution of $^{208}Pb/^{232}Th$ ages and confirm the presence of inherited Pb in this sample. Although in this case it is not possible to unambiguously resolve inherited component(s), con-

sidering our monazite ages and other published isotopic studies on this sample, the best current estimate of the crystallization age of Rongbuk is $22^{+1.0}_{-0.5}$ Ma. These data provide timing constraints on the termination of slip on the North Himalayan fault, and indicate that the Main Central thrust was active at 23 ± 1 Ma.

Acknowledgements

We thank G. Gehrels, R. Parrish, F. Corfu, and J.-M. Montel for providing us with monazite standards and unpublished data; and R. Parrish, K. Hodges, and T. Ireland for helpful reviews. This research was supported by grants from the National Science Foundation. We particularly wish to thank the directors and staff of the W.M. Keck Foundation for their generous support. [*PT*]

References

[1] P. LeFort, M. Cuney, C. Deniel, C. France-Lanord, S.M.F. Sheppard, B.N. Upreti and P. Vidal, Crustal generation of the Himalayan leucogranites, Tectonophysics 134, 39–57, 1987.

[2] P. Vidal, Rb–Sr systematics in granite from central Nepal (Manaslu): significance of the Oligocene age and high $^{87}Sr/^{86}Sr$ ratio in Himalayan orogeny, Comment, Geology 6, 196, 1978.

[3] C. France-Lanord, S.M. Sheppard and P. LeFort, Hydrogen and oxygen isotope variations in the High Himalaya peraluminous Manalsu leucogranite: Evidence for heterogeneous sedimentary source, Geochim. Cosmochim. Acta 52, 513–526, 1988.

[4] C. France-Lanord and P. LeFort, Crustal melting and granite genesis during the Himalayan collision orogenesis, Trans. R. Soc. Edinburgh 79, 183–196, 1988.

[5] P. LeFort, Manaslu leucogranite: A collision signature of the Himalaya, a model for its genesis and emplacement, J. Geophys. Res. 86, 10,545–10,568, 1981.

[6] P. Vidal, J. Benard-Griffiths, A. Cocherie, P. Le Fort, J.J. Peucatt and S.M.F. Sheppard, Geochemical comparison between Himalayan leucogranites, Phys. Earth Planet. Inter. 35, 179–190, 1984.

[7] P. LeFort, A. Pêcher and P. Vidal, Les gneiss oeillès de la Dalle du Tibet: un episode magmatique au Palèozoique infèrieur en Himalaya du Népal, in: 9e Reunion Ann. Sci. Terre, Paris, 1982.

[8] P. Vidal, A. Cocherie and P. LeFort, Geochemical investigations of the origin of the Manaslu leucogranite (Himalaya, Nepal), Geochim. Cosmochim. Acta 46, 2279–2292, 1982.

[9] C. Deniel, P. Vidal, A. Fernandez, P. Le Fort and J.J. Peucat, Isotopic study of the Manaslu granite (Himalaya, Nepal): inferences on the age and source of the Himalayan leucogranites, Contrib. Mineral. Petrol. 96, 78–92, 1987.

[10] A. Pêcher, The contact between the higher Himalaya Crystallines and the Tibetan Sedimentary Series: Miocene large-scale dexteral shearing, Tectonics 10, 587–598, 1991.

[11] P. Copeland, T.M. Harrison and P. LeFort, Age and cooling history of the Manaslu granite: Implications for Himalayan tectonics, J. Volcanol. Geotherm. Res. 44, 33–50, 1990.

[12] S. Guillot, K.V. Hodges, P. LeFort and A. Pêcher, New constraints on the age of the Manaslu leucogranite: Evidence for episodic tectonic denudation in the central Himalaya, Geology 22, 559–562, 1994.

[13] S. Guillot, A. Pêcher, P. Rochette and P. LeFort, The emplacement of the Manaslu granite of central Nepal: field and magnetic susceptibility constraints, in: Himalayan Tectonics, M.P. Searle and P.J. Treloar, eds., Geol. Soc. London Spec. Publ. 74, 413–428, 1993.

[14] C.H. Chen and D.J. DePaolo, Rb–Sr microchrons in the Manaslu Granite: Implications for Himalayan thermochronology, EOS 73, 545, 1992.

[15] J.P. Burg, M. Brunel, D. Gapais, G.M. Chen and G.H. Liu, Deformation of leucogranites of the crystalline Main Central Sheet in southern Tibet (China), J. Struct. Geol. 6, 535–542, 1984.

[16] B.C. Burchfiel and L.H. Royden, North–south extension within the convergent Himalayan region, Geology 13, 679–682, 1985.

[17] B.C. Burchfiel, Chen Z., K.V. Hodges, Liu Y., L.H. Royden, Deng C. and Xu J., The South Tibetan Detachment System, Himalayan Orogen: Extension contemporaneous with and parallel to shortening in a collisional mountain belt, Geol. Soc. Am. Spec. Pap. 269, 41 pp., 1992.

[18] K.V. Hodges, R.R. Parrish, T.B. Housh, D.R. Lux, B.C. Burchfiel, L.H. Royden and Chen Z., Simultaneous Miocene extension and shortening in the Himalayan orogen, Science 258, 1466–1470, 1992.

[19] M.S. Hubbard and T.M. Harrison, $^{40}Ar/^{39}Ar$ age constraints on deformation and metamorphism in the MCT Zone and Tibetan Slab, eastern Nepal Himalaya, Tectonics 8, 865–888, 1989.

[20] R.R. Parrish and K.V. Hodges, Miocene (22 ± 1) Ma metamorphism and two stage thrusting in the Greater Himalayan Sequence, Annapurna Sanctuary, Nepal, Geol. Soc. Am. Abstr. Prog. 25, A174, 1993.

[21] C.F. Miller, E.B. Watson and T.M. Harrison, Perspectives on the source, segregation and transport of granitoid magmas, Trans. R. Soc. Edinburgh 79, 135–156, 1988.

[22] T.M. Harrison and E.B. Watson, Kinetics of zircon dissolution and zirconium diffusion in granitic melts of variable water content, Contrib. Mineral. Petrol. 84, 66–72, 1983.

[23] J.-M. Montel, A model for monazite/melt equilibrium and application to the generation of granitic magmas, Chem. Geol. 119, 127–146, 1993.

[24] P. Copeland, R.R. Parrish and T.M. Harrison, Identification of inherited radiogenic Pb in monazite and its implications for U–Pb systematics, Nature 333, 760–763, 1988.

[25] U. Schärer, The effect of initial ^{230}Th disequilibrium on young U–Pb ages: The Makalu case, Earth Planet. Sci. Lett. 67, 191–204, 1984.

[26] W. Compston, I.S. Williams and C. Meyer, U–Pb geochronology of zircons from Lunar Breccia 73217 using a sensitive, high mass resolution ion microprobe, J. Geophys. Res. 89, 8525–8534, 1984.

[27] J.-M. Montel, F. Lhote and J.M. Claude, Monazite and end members and solid solutions: synthesis, unit-cell characteristics, and utilization as microprobe standards, Mineral. Mag. 53, 120–123, 1989.

[28] L.A. Boatner and B.C. Sales, Monazite, in: Radioactive Waste Forms for the Future, W. Lutze and R.C. Ewing, eds., pp. 495–564, Elsevier, Amsterdam, 1988.

[29] M. Schuhmacher, E. de Chambost, K.D. McKeegan, T.M. Harrison and H. Migeon, In situ dating of zircon with the CAMECA ims 1270, in: Secondary Ion Mass Spectrometry SIMS IX, A. Benninghoven et al., eds., pp. 919–922, 1994.

[30] F. Corfu, Differential response of U–Pb systems in coexisting accessory minerals, Winnepeg River Subprovince, Candian Shield: Implications for Archean crustal growth and stabilization, Contrib. Mineral. Petrol. 98, 312–325, 1988.

[31] M.K. Roden, R.R. Parrish and D.S. Miller, The absolute age of the Eifelian Tioga ash bed, Pennsylvania, J. Geol. 98, 282–285, 1990.

[32] D.A. Foster, Mesozoic and Cenozoic thermal history of the eastern Mojave Desert, California, and western Arizona, with emphasis on the Old Woman Mountains area and the Chemehuevi Metamorphic Complex, Ph.D. thesis, SUNY, Albany, NY, 1989.

[33] T.M. Harrison and K.I. Mahon, New constraints on the age of the Manaslu leucogranite: Evidence for episodic tectonic denudation in the central Himalaya: Comment, Geology 23, 478–479, 1995.

[34] B. Scallet, M. Pichavant and J. Roux, Experimental crystallization of leucogranite magmas, J. Petrol. 36, in press, 1995.

[35] R.R. Parrish, U–Pb dating of monazite and its application to geological problems, Can. J. Earth Sci. 27, 1431–1450, 1990.

[36] R.R. Parrish and S.D. Carr, U–Pb problematics of very high-U accessory minerals: Examples from the Himalaya and Cordillera and implications for U–Pb geochronology, US Geol. Surv. Circ. 1107, 243, 1994.

[37] Le Fort, P., Himalayas, the collided range. Present knowledge of the continental arc, Am. J. Sci. 275A, 1–44, 1975.

[38] A. Yin, T.M. Harrison, F.J. Ryerson, W. Chen, W.S.F. Kidd and P. Copeland, Tertiary structural evolution of the Gangdese thrust system, southeastern Tibet, J. Geophys. Res. 99, 18,175–18,201, 1994.

[39] P. Copeland, T.M. Harrison, R.R. Parrish, B.C. Burchfiel, K. Hodges and W.S.F. Kidd, Constraints on the age of normal faulting, north face of Mt. Everest: Implications for Oligo-Miocene uplift, EOS 68, 1444, 1987.

[40] T.M. Harrison and J.D. Fitzgerald, Exsolution in hornblende and its consequences for ^{40}Ar/^{39}Ar age spectra and closure temperature, Geochim. Cosmochim. Acta 50, 247–253, 1986.

[41] S.L. Baldwin, T.M. Harrison and J.D. Fitz Gerald, Diffusion of ^{40}Ar/^{39}Ar in metamorphic hornblende, Contrib. Mineral. Petrol. 105, 691–703, 1990.

[42] A. Yin, Mechanics of wedge-shaped blocks I: an elastic solution for compresional wedges, J. Geophys. Res. 98, 14,245–14,256, 1993.

[43] N. Harris and J. Massey, Decompression and anatexis of Himalayan metapelites, Tectonics 13, 1537–1546, 1994.